



1 **Associations of interannual variation of Summer Tropospheric Ozone with**
2 **Western Pacific Subtropical High in China from 1999 to 2017**

3
4 **Authors:** Xiaodong Zhang^{1,#}, Ruiyu Zhugu^{1,#}, Xiaohu Jian¹, Xinrui Liu¹, Kaijie Chen¹,
5 Shu Tao¹, Junfeng Liu¹, Hong Gao², Tao Huang², Jianmin Ma^{1,*}

6
7 **Affiliations:**

8 ¹Laboratory for Earth Surface Processes, College of Urban and Environmental Sciences,
9 Peking University, Beijing 100871, China

10 ²Key Laboratory for Environmental Pollution Prediction and Control, College of Earth
11 and Environmental Sciences, Lanzhou University, Lanzhou 730000, China

12
13 # These authors contribute equally to this article

14 * Corresponding author. E-mail address: jmma@pku.edu.cn (J.M. Ma).

15
16 **Abstract**

17 Associations between tropospheric ozone (O₃) and climate variations have been
18 extensively investigated worldwide. However, given the lack of historical O₃
19 monitoring data, the knowledge gaps regarding the influences of climate variations on
20 long-term O₃ trends in China remain. The present study used a unique tropospheric O₃
21 dataset from the summer of 1999 to 2017 simulated by an atmospheric chemistry model
22 to explore the linkage between summer O₃ and a dominant atmospheric circulation
23 system – the Western Pacific Subtropical High Pressure (WPSH) on an interannual
24 basis in China. During this period, both WPSH strength and O₃ concentrations in
25 eastern and central China illustrated a growing trend. An EOF analysis was conducted
26 to examine significant summer O₃ characteristics and patterns and their potential
27 connections with the WPSH. We show that the WPSH determines interannual
28 fluctuations of summer O₃, whereas O₃ precursor emissions contribute primarily to the
29 O₃ long-term trend. Special efforts were made to discern the associations of O₃
30 variations in major urban agglomerations of China and the WPSH. The results reveal
31 that the WPSH plays a more vital role in O₃ perturbation in the eastern seaboard regions



32 and inland China, but leads to lower O₃ levels in the Pearl River Delta (PRD) region.
33 Precursor emissions made more significant contributions up to 60% to increasing O₃
34 trends in the inland urban agglomerations than coastal regions in eastern and southern
35 China. The strongest contribution of meteorological conditions associated with the
36 WPSH to summer ozone concentration occurred in the Yangtze River Delta (YRD),
37 accounting for over 9% to ozone perturbations from 1999 to 2017. Overall, we find that
38 the effect of the WPSH on regional O₃ depends on the spatial proximity to the WPSH.
39 We attributed the effects of the WPSH on O₃ interannual variations to the changes in
40 air temperature, precipitation, and winds associated with the WPSH's intensity and
41 positions.

42 **Keywords:** tropospheric ozone, western pacific subtropical high, climate, EOF analysis
43

44 1. Introduction

45 Tropospheric (or surface) ozone is one of the most important components of
46 atmospheric chemistry and is also a prominent atmospheric pollutant in China in recent
47 years (Ma et al., 2021). Ground-level ozone pollution has overtaken PM_{2.5} as the
48 leading pollutant in many of China's urban and industrial regions (Lu et al., 2018).
49 Surface ozone is produced through the photochemical oxidation of carbon monoxide
50 (CO) and volatile organic compounds (VOCs) in the presence of nitrogen oxides (NO_x)
51 and sunlight (Akimoto et al., 2015; Liu and Wang, 2020; Lu et al., 2018; Ma et al.,
52 2021). Unlike stratospheric ozone, which absorbs harmful UV radiation that could
53 otherwise reach the Earth's surface and cause adverse health impacts on humans,
54 surface ozone has detrimental effects on both human health and terrestrial vegetation
55 (Fleming et al., 2018; Lefohn et al., 2017; Liu et al., 2018; Liu and Wang, 2020).
56 Extensive studies have revealed significant associations between short-term or acute
57 exposure to ozone concentrations and respiratory and cardiovascular morbidity,
58 inhibiting lung development, new onset asthma, hospital admissions, and premature
59 mortality (Bell et al., 2014; Fleming et al., 2018; Yan et al., 2013). It is estimated that



60 death related to ozone exposure comprises 5–20% of all those caused by air pollution
61 (Brauer et al., 2012; Monks et al., 2015; Silva et al., 2013). In the past decade, partly
62 due to rapid economic growth and urbanization in China, surface O₃ has increased
63 dramatically (Maji et al., 2019; Zhan et al., 2018). Many urban areas across China have
64 experienced growing ozone pollution, despite implementing various stringent emission
65 reduction measures since 2013 (Bell et al., 2014; Liu and Wang, 2020; Yan et al., 2013).
66 Although the median ozone values exhibit no significant disparity between China and
67 many industrialized countries and regions such as Japan, South Korea, Europe, and the
68 United States (US), the frequency of high-ozone events in China is much higher than
69 those developed countries and regions (Lu et al., 2018; Ma et al., 2016; Xu et al., 2016).

70 Surface ozone formation and evolution rely on meteorology, atmospheric
71 chemistry, and the emissions of O₃ precursors, such as VOCs and NO_x emitted from
72 fuel combustion (Li et al., 2020; Ma et al., 2021). Meteorological parameters affecting
73 surface O₃ evolution include but are not limited to winds, air temperature, relative
74 humidity, and solar radiation (Ma et al., 2021). While anthropogenic factors play vital
75 roles in ozone formation, meteorological factors determine, to a significant extent, the
76 changes and evolution in O₃ concentrations (Ding et al., 2019; Li et al., 2019, 2020; Lin
77 et al., 2021, 2022). Meteorological conditions modulate O₃ concentrations through
78 atmospheric transport and affect natural emissions from biological sources and
79 chemical reaction rates (Fu et al., 2019; Li et al., 2020; Lu et al., 2019). Extensive
80 investigations have been devoted to short-term, such as hourly and diurnal changes in
81 O₃ levels and their associations with meteorological conditions (Dang et al., 2021; Han
82 et al., 2020). Given the strong connections between O₃ concentration and air
83 temperature, atmospheric humidity, and winds, interannual and longer-term variations
84 of O₃ are also elucidated in China and worldwide (Chen et al., 2020; Li et al., 2020).
85 Daily and interannual variations of summertime surface O₃ have been linked with
86 atmospheric teleconnection patterns, such as the ENSO (El Niño-Southern Oscillation),
87 East Asian summer monsoon, and the WPSH (Liu et al., 2019a; Wang et al., 2016;
88 Yang et al., 2022; Yihui and Chan, 2005; Yin et al., 2019; Zhao and Wang, 2017; Zhou
89 et al., 2009). These climate teleconnection patterns provide dynamic and



90 thermodynamic backgrounds of regional and large-scale weather systems that could
91 markedly affect the atmospheric pressure, temperature, and winds. Using modeled O₃
92 time series across China from 1999 to 2017, we have examined the response of gridded
93 summer O₃ concentrations to the East Asian Summer Monsoon Index (EASMI), Nino
94 indices, and western North Pacific subtropical high index (WPSH-I) on an annual basis
95 in the six major urban agglomerations in China (UAs, Zhang, et al., 2022). The results
96 revealed that interannual changes in summer O₃ in these UAs were more significantly
97 associated with the WPSH-I among these atmospheric teleconnection patterns. The
98 finding motivates us to carry out more broad and deep investigations of the associations
99 between the long-term change in summer O₃ and the WPSH, aiming to shed new light
100 on the extent of the impact of climate variation on O₃ trends in urban China.

101 Limited studies have been carried out to examine the linkage of summer O₃ in
102 China with the WPSH (Jiang et al., 2021; Yin et al., 2019; Zhao and Wang, 2017; Liu
103 et al., 2019a). These studies all focused on the response of daily summer O₃ variation
104 to the WPSH in eastern China using measured O₃ concentrations within a short period
105 (e.g., 2015-2018, Yin et al., 2019) rather than interannual or longer ozone trends in
106 mainland China. To fill this knowledge gap, we performed multiple atmospheric
107 chemistry model simulations of summer (June, July, and August) O₃ concentrations
108 across China from 1999 to 2017. This unique O₃ dataset enables us to explore the
109 responses of the long-term trend and interannual variation of O₃ concentrations to
110 climate variations and to take a broader look at the associations between ozone
111 evolution and the Western Pacific subtropical high in China (Zhang et al., 2022).

112 **2. Methodology**

113 **2.1. WRF-Chem Model Configuration**

114 The Weather Research and Forecasting model coupled with Chemistry (WRF-
115 Chem) v3.7 (http://www2.mmm.ucar.edu/wrf/users/wrf_files/wrfv3.7/updates-3.7.html) was employed to quantify the influences of the WPSH on O₃ variation in
116 China. The model covers mainland China with a 20 km × 20 km grid resolution,
117



118 extending from the ground surface to 50 hPa with 30 non-uniformly distributed verticle
119 layers (Zhang et al., 2022). Anthropogenic emissions data of atmospheric pollutants
120 from 1998 to 2017 were collected from EDGAR (Emissions Database for Global
121 Atmospheric Research) v4.3 (<https://edgar.jrc.ec.europa.eu/>), including gridded annual
122 emission data for CH₄, BC, OC, NH₃, NMVOC, NO_x, CO, SO₂, and primary PM₁₀ and
123 PM_{2.5}. The biogenic emissions were estimated by the MEGAN v2.1 (Model of
124 Emissions of Gases and Aerosols from Nature) (Guenther et al., 2012). Detailed WRF-
125 Chem configuration, modeling setup, and precursor emissions are referred to by Zhang
126 et al. (2022). WRF-Chem model was integrated to predict daily O₃ concentrations in
127 summer (June to August) from 1998 to 2017. After excluding the model spin-up time,
128 the O₃ time series from 1999 to 2017 was used in the present study. The daily
129 concentrations were summed and averaged over the summer season to obtain mean O₃
130 concentrations. The modeled O₃ concentrations were verified by measured O₃
131 concentration data in several major urban agglomerations across China. More details
132 are referred to in Supporting Information Text 1 and **Fig. S1**.

133 **2.2. WPSH index**

134 The WPSH indices were collected from the National Climate Center of China
135 (NCCC, the WPSH index is available at [http://cmdp.ncc-](http://cmdp.ncc-cma.net/download/precipitation/diagnosis/NWP_high/wpsh_idx.txt)
136 [cma.net/download/precipitation/diagnosis/NWP_high/wpsh_idx.txt](http://cmdp.ncc-cma.net/download/precipitation/diagnosis/NWP_high/wpsh_idx.txt)). The NCCC
137 reports four WPSH indices, including the WPSH area index, intensity index, the
138 westernmost point, and the ridgeline index of the WPSH. These indices define and
139 quantify the changes in the WPSH via its size, intensity, east–west expansion, and
140 north–south movement (Liu et al., 2019b). These WPSH activities significantly affect
141 China's daily, seasonal, interannual, and longer-term meteorological fields and climate
142 variations. Among the four WPSH indices, we found that the WPSH area index
143 (hereafter referred to as WPSH-II) exhibited the most significant positive correlations
144 with modeled summer ozone concentrations in most regions of China. The strongest
145 negative correlations occur between O₃ concentrations and the westernmost point of the



146 WPSH (hereafter referred to as WPSH-I2). In light of this, we chose the WPSH-I1 and
147 WPSH-I2 to elucidate the potential influences of the WPSH on the interannual
148 variations of WRF-Chem simulated summer O₃ concentrations for the past two decades.
149 As shown in **Fig. S2**, the WPSH strength characterized by the WPSH-I1 index
150 illustrates a growing trend after 1999, suggesting the reinforcement of the WPSH on a
151 decadal scale in the recent two decades, the period coincident with the most rapidly
152 growing O₃ pollution in China. This trend possibly overwhelms interannual changes in
153 the WPSH in the recent two decades.

154 **2.3. O₃ data**

155 Surface O₃ concentration data on a daily basis used the WRF-Chem simulated
156 concentration data (section 2.1). Meteorological data used the WRF predicted gridded
157 air temperature (C°), 500-hPa geopotential height (GH, ghm), winds, and the sea
158 surface pressure (SSP, hPa). To perform the composite analysis for examining the
159 responses of interannual variation of summer ozone to the WPSH, we also collected
160 geopotential height at the 500 hPa, the surface air temperature (°C), and precipitation
161 from NCEP reanalysis (<https://psl.noaa.gov/data/reanalysis/reanalysis.shtml>). These
162 data were used to illustrate the characteristics of meteorological fields during the
163 positive and negative phases of WPSH indices and in the first EOF loadings, which will
164 be elaborated on below.

165 **2.4. EOF analysis**

166 To extract the potential influences of the interannual changes in the WPSH on O₃
167 variations, we conducted the EOF analysis and examined associations between
168 meteorological fields and surface O₃ from 1999 to 2017, respectively. The empirical
169 orthogonal function (EOF) analysis as a multivariate statistical technique has been
170 extensively used in atmospheric science to explore the spatiotemporal variations in a
171 meteorological variable or air pollutant (Fiore et al., 2003; Pu et al., 2016; Shen et al.,
172 2015; Yin et al., 2019; Zhao and Wang, 2017). In the present study, we used the EOF



173 analysis in WRF-Chem simulated gridded (20 km × 20 km) seasonal O₃ concentrations
174 across China to extract annual O₃ change features from 1999 to 2017, respectively. The
175 EOF analysis of the O₃ concentration time series from modeled data was designed to
176 investigate potential associations between the summer O₃ time series and WPSH and
177 to explore the response of the O₃ time series to increasing WPSH strength since 1999.
178 The orthogonal modes included spatial and temporal coefficients and contained
179 information of some proportion (variance contributions) from the original fields.

180 2.5. Model scenario setup

181 We quantify the contribution of meteorology and precursor emissions to O₃
182 evolution subject to WPSH by setting up three model scenarios. Considering the
183 increasing trend of the WPSH from 1999 onward, we integrated WRF-Chem from 1998
184 to 2017, subject to three model runs. The first model scenario run took the variable
185 meteorological field and annual O₃ precursor emissions from 1998 to 2017, with 1998
186 as the model spin-up period, referred to as the base scenario (scenario 1); the second
187 scenario run adopted fixed precursor emissions in 1998, but variable meteorology
188 throughout 1998 to 2017, referred to as model scenario 2, and the third scenario
189 implemented fixed meteorology in 1998 but variable precursor emissions, referred to
190 as model scenario 3. The simulated O₃ concentrations from these three scenarios were
191 compared to identify the relative significance of meteorology and precursor emissions
192 in the changes in O₃ concentrations.

193

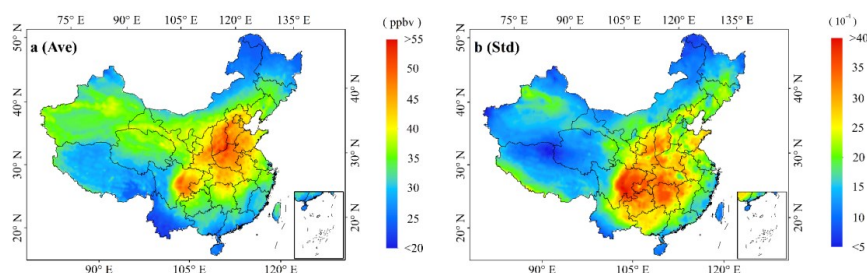
194 3. Results and Discussion

195 3.1. EOF analysis

196 **Figures 1a** and **1b** show modeled summer mean O₃ concentrations and standard
197 deviations (STD) averaged from 1999 to 2017. Higher concentrations are observed in
198 Sichuan and the region extending from central China to the Northern China Plain (NCP),
199 rather than the southern and southeastern seaboard areas where O₃ pollution has been



200 receiving extensive concerns (**Fig. 1a**). This spatial distribution pattern agrees well with
201 measured mean summer concentrations data averaged from 2015 to 2017 in China (**Fig.**
202 **S3**). The STD distribution does not superimpose with O₃ concentrations but is centered
203 in the Sichuan Basin and those provinces in the middle reaches of the Yangtze River,
204 implying that O₃ fluctuated more strongly by interannual variations of meteorological
205 fields in this region.
206

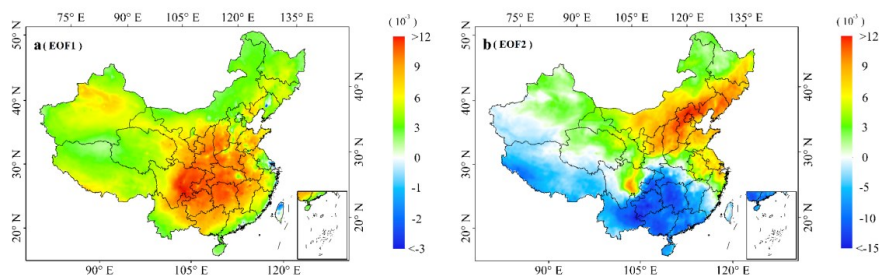


207
208 **Figure 1.** Mean summer O₃ concentrations (**a**) and standard deviations (**b**) averaged from 1999 to
209 2017.

211 We carried out an EOF analysis by using summer O₃ as the original field to
212 illustrate the spatiotemporal variation of O₃ in China on an annual basis from 1999 to
213 2017, aiming to explore the response of summer O₃ interannual (1999 to 2017) variation
214 to the WPSH, the period matching the significantly increasing trend of the WPSH-II
215 (Supporting Information (SI), Inset figure of **Fig. S2**), which may lead to a more robust
216 response of the O₃ time series to the WPSH. The results of the first and second EOF
217 patterns for both periods are presented in **Fig. 2**. Each EOF spatial pattern represents a
218 share of the total variation of surface ozone proportional to its eigenvalue. The first
219 EOF loadings (PCA1) are associated strongly with the mean summer O₃ concentrations
220 averaged over the six UAs in China at the correlation coefficient of 0.95 ($p < 0.01$) from
221 1999 to 2017. The EOF1 pattern also illustrates similarities with the mean summer O₃
222 concentrations and its standard deviations (**Fig. 1a** and **1b**), featured by large values in
223 central China. Differing from the EOF1, the EOF2 patterns show a south-north contrast
224 pattern. During this period, the first EOF pattern (EOF1) explains 67.4% of the total
225 variance in summer O₃, and the second EOF pattern (EOF2) explains 9.7% of the total



226 variance. The negative and positive values in the EOF patterns are expected to represent
 227 the extent of departures from the average summer ozone. Since the EOF1 pattern is the
 228 maximum possible fraction of the variability in the original data, in our case, it explains
 229 most of the summer O₃ variability, featured by the growing trends of summer O₃
 230 concentrations. The EOF1 pattern appears to agree, to a large extent, with measured
 231 summer (June to August) and warm season (April to September) MDA8 (maximum 8h
 232 average) O₃ distribution (Lu et al., 2018; Liu, 2020). The EOF2 patterns also agree with
 233 the second EOF pattern that Yin et al. (2019) obtained, though their EOF analysis
 234 focused on daily O₃ in eastern China. The result suggests that the NCP suffered from
 235 higher O₃ pollution and was also subject to O₃ evolution during the past decades.
 236



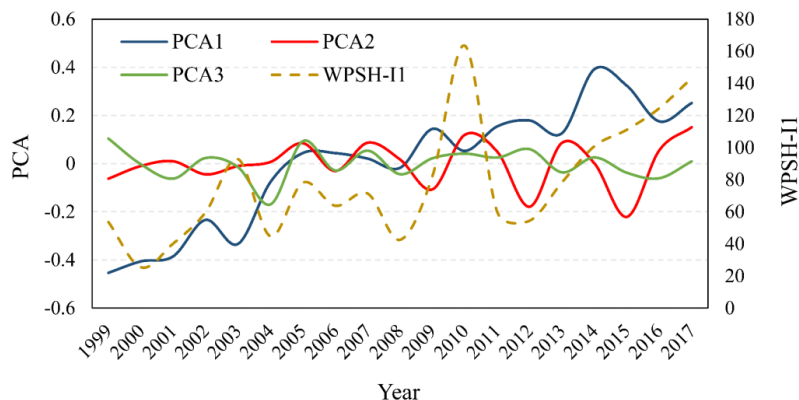
237
 238 **Figure 2.** First (a) and second (b) EOF patterns across China from 1999 to 2017.

239
 240 The EOF1 shown in **Figs. 2a** suggests that the most significant variations in
 241 summer O₃ occurred in inland areas of China, extending from Sichuan Province to the
 242 middle and lower reaches of the Yangtze River and from Hunan to Shanxi Province.
 243 This inland region covers several major urban agglomerations (UAs) in China,
 244 including Central China (CC), Middle Reaches of the Yangtze River (MYR), and
 245 Chengyu (CY, Chengdu–Chongqing) urban agglomeration (Zhang et al., 2022). We
 246 estimated the correlation coefficients between the first EOF loading (PCA1) and
 247 summer O₃ concentrations in the six UAs, where 34.3% of China's population resides.
 248 The results are presented in **Fig. S4**. Strong statistically significant correlations were
 249 found in CC ($r = 0.86, p < 0.01$), CY ($r = 0.92, p < 0.01$), and MYR ($r = 0.90, p < 0.01$).
 250 Whereas, in the other three UAs located near the coastal regions, namely the YRD,



251 PRD, and BTH, the correlation coefficients range from 0.36 to 0.51 (**Fig. S4**). In
 252 particular, the PCA1 exhibits more strong association with the summer O₃ anomalies
 253 averaged over the six UAs, reaching $r=0.94$ ($p<0.01$). The good correlations between
 254 O₃ concentrations and PCA1 are expected because, as aforementioned in section 3.1
 255 that, the EOF analysis was carried out by using summer O₃ concentrations as the
 256 original field that have been increasing during the past decades. However, the
 257 magnitude of the correlation coefficients helps identify the extent of O₃ pollution and
 258 long-term growth trends in China and different UAs (or regions). Overall, these results
 259 confirm a more substantial interannual variation of summer O₃ in the inland areas than
 260 in coastal regions of southern and southeastern China.

261



262

263 **Figure 3.** Annual variation of three EOF loadings (PCA1-3, scaled on the left Y-axis) and WPSH-
 264 II (dashed brown line, scale on the right Y-axis) from 1999 to 2017.

265

266 **Figure 3** shows annual variations of the three EOF loadings (PCA1-3), scaled on
 267 the left Y-axis) and the WPSH-II (dashed brown line, scaled on the right Y-axis) from
 268 1999 to 2017. The first EOF loading (PCA1) and WPSH-II exhibit growing trends
 269 during this period with a correlation coefficient of 0.56 ($p<0.01$). The increasing trend
 270 of WPSH-II since 1999 likely anticipates the interdecadal variation of the WPSH for
 271 the recent two decades. Since O₃ concentrations are positively correlated with the
 272 WPSH-II (**Figs. 3-5**), stronger WPSH intensity might elevate summer O₃ levels in
 273 China on an annual basis, particularly the areas with large EOF1 values in inland China



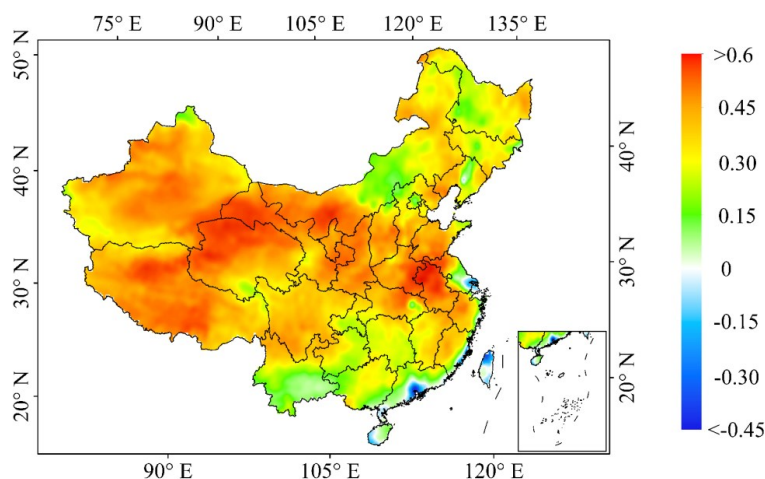
274 (**Fig. 2a**). However, this conclusion is not well applicable in the PRD region, where we
275 observed the lowest association between the EOF1 and summer O₃ concentrations (**Fig.**
276 **2**) and between the WPSH-II and O₃ levels among the six UAs and over China (**Fig.**
277 **S4**). It is also worthwhile to note that, because O₃ precursor emissions in China have
278 been growing during the past two decades and modeled concentrations were mainly
279 attributed to precursor emissions, the positive correlations between O₃ concentrations
280 and the WPSH-II should not be understood that the WPSH drove elevated O₃ for a
281 long term perspective. Further discussions are provided in the next section.

282 We further compared the 500-hPa geopotential heights (GH, gpm) anomalies in
283 the positive and negative phases of PCA1 and WPSH-II as the departure from their
284 respective means averaged from 1999 to 2017. We selected those years with the
285 positive and negative anomalies of the PCA1 and WPSH-II $\geq \pm 1$ standard deviation
286 (STD, referred to as the positive and negative phase hereafter) and then estimated their
287 composite means. The results are shown in **Figs. S5** and **S6**. It can be seen that the
288 composite means of 500-hPa geopotential height in the positive and negative phases of
289 the PCA1 and WPSH-II illustrate good spatial similarities, again demonstrating the
290 connections between summer O₃ and WPSH-II. In the positive phase, positive
291 geopotential height anomalies at the 500-hPa governed China, except for the NCP
292 regions, including the BTH urban agglomeration, where negative anomalies of the 500-
293 hPa geopotential heights are observed. On the other hand, a south-north contrast pattern
294 of the geopotential height composite anomalies is discerned in the negative phase of
295 the PCA1 and WPSH-II. The spatial patterns of GH composite anomalies in the
296 positive and negative phases of the EOF1 also exhibit some similarities with the GH
297 composite anomalies based on positive and negative O₃ concentration anomalies as the
298 departure from mean O₃ levels averaged over the six UAs in China from 1999 to 2017
299 (**Fig. S6**).

300 **3.2. Associations of summer O₃ with WPSH**



301 Having established the relationships between summer O₃ and WPSH via the EOF
302 analysis, we further explore the direct responses of summer O₃ to WPSH. Since the
303 effects of the WPSH span vast regions, and the changes in surface ozone concentrations
304 may be influenced by the variations in meteorological factors associated with the
305 WPSH, a spatial correlation analysis between summer surface ozone concentrations in
306 China and WPSH (WPSH-II) index from 1999 to 2017 was conducted. The result is
307 illustrated in **Fig. 4**. During this period, positive correlations overwhelm mainland
308 China, except for the PRD region (**Fig. 4**). Surprisingly, the negative correlations in the
309 PRD region might suggest that the stronger WPSH tends to reduce the summer O₃ in
310 this well-developed and populated UA in China, as aforementioned above. The summer
311 O₃ level in the PRD was the lowest among the six UAs (**Figs. 1 and S3**). No statistically
312 significant O₃ trend was identified in the PRD, likely attributed to O₃ pollution control
313 in the early 2000s under the joint efforts from Hong Kong and Guangdong provincial
314 governments to improve the air quality in the PRD and Hong Kong (Wu et al., 2013).
315 We also estimated the correlations between O₃ concentrations averaged over the six
316 UAs across China and the WPSH-II from 1999 to 2017 (**Fig. S7**). The positive
317 correlation coefficients between the mean O₃ concentrations and the WPSH-II in each
318 of the UAs are presented at the top of each column. The results suggest that increasing
319 WPSH-II plays a specific role in elevated O₃ levels in eastern China and these UAs.
320 Again, as aforementioned, a decadal scale-increasing WPSH-II trend occurred since
321 the late 1990s and early 2000s (**Fig. S1**), which seems coincident with the rapidly
322 increasing O₃ precursor emissions and concentration trends in China and its major
323 urban areas (Liu and Wang, 2020; Lu et al., 2018). Hence, the positive correlations
324 between the summer WPSH-II and O₃ concentrations might not be attributable, to a
325 large extent, to growing O₃ pollution. Further discussions are presented in section 3.3.
326



327

328 **Figure 4.** Correlation coefficients between summer O₃ concentrations and WPSH-I1 across China
329 from 1999 to 2017 on the interdecadal scale.

330

331

332 Considering that summer precipitation in China is sensitive to the western ridge
333 point of the WPSH, we also examined the responses of meteorological fields to the
334 changes in the western ridge point index of the WPSH (referred to as the WPSH-I2)
335 subject to its positive and negative phases. The WPSH-I2 is opposite to the WPSH-I1
336 (**Fig. S8**). We estimated WPSH-I2 anomalies as the departure from its mean from 1999
337 to 2017. We defined the positive WSH-I2 phase if its values are greater than one
338 standard deviation and the negative phase if WSH-I2 < one standard deviation. The
339 annual summer mean meteorological variables in the positive and negative phases of
340 the WSH-I2 are summed to obtain their respective composite means. We then
341 calculated the anomalies of these composite means by subtracting their respective long-
342 term means averaged from 1990 to 2022. **Figure 5** shows the anomalies of composite
343 means of 500-hPa GH, precipitation (cm/mn), and the surface air temperature (SAT,
344 °C) across China in the positive and negative phases of WPSH-I2. The results identified
345 evident north-south contrast for all three meteorological variables in the positive phase
346 of the WPSH-I2. Of which, the anomalies of GH composite means are positive in
347 northern China with a center in Mongolia and northeastern China (**Fig. 5a**). In contrast,



348 the broad region to the south of 35°N is under the regime of negative GH composite
349 anomalies (**Fig. 5b**). The 500-hPa GH patterns can also be confirmed by the anomalies
350 of composite mean sea level pressure (SLP) in the positive and negative phase of
351 WPSH-I2 (**Fig. 6**), showing negative SLP anomalies from the Bay of Bengal to the
352 tropical western Pacific in the positive phase of the WPSH-I2 and positive anomalies
353 covering a vast region from southeast to northeast China. The south-north dipole
354 patterns of 500-hPa GH composite anomalies in **Fig. 5a** and the SLP composite
355 anomalies in **Fig. 6** often accompany the termination of the rain season in southern
356 China and the start of the rainy season in northern China (Nie et al., 2021), as shown
357 by the negative rainfall anomaly in southern China and positive anomaly in northern
358 China. **Figure 5a** predicts the weakening WPSH or the northward movement of the
359 WPSH, leading to a southward pressure gradient, as shown in **Fig. 5a**. As a result, the
360 composite anomalies of 850-hPa vector winds illustrate northerly wind components
361 over central-south and southern China (**Fig. 6**). Such northerly wind anomalies do not
362 favor southward water vapor transport by southwesterly Indian monsoon.

363 On the other hand, easterly and southeasterly wind components extend from
364 tropical west Pacific to central and northern China, paving a water vapor transport
365 pathway and corresponding to the positive rainfall anomaly in this part of China (**Fig.**
366 **5c**). In the negative phase of the WPSH-I2, positive SLP anomalies overwhelmed
367 eastern China with a center in the coastal region of southern China, implying the
368 enhancement of the WPSH. Accordingly, we observe negative composite anomalies of
369 the precipitation extending from the Yangtze-Huaihe Valley from central to
370 northeastern China, suggesting declining precipitations in these regions. Growing
371 precipitations are seen in southern and southeastern China, characterized by the positive
372 composite anomalies of the precipitation (**Fig. 5c**).

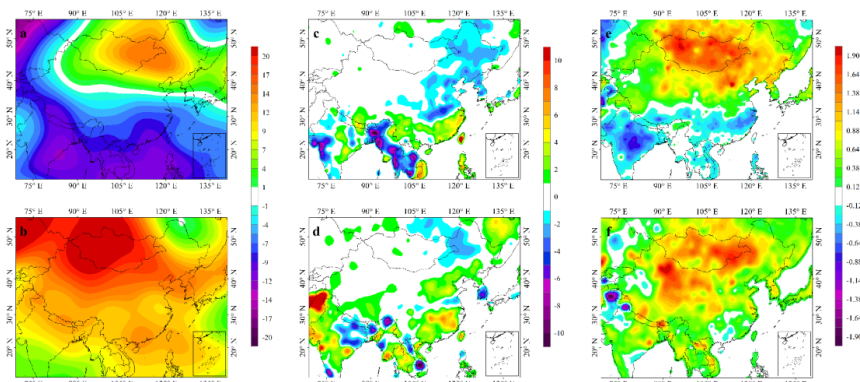
373 Precipitations in China have been connected strongly with the WPSH-I2 from a
374 daily perspective (Duan et al., 2008; Nie et al., 2021). Along with the westward shifting
375 of the WPSH ridge point, the major rain belt moves northward to the middle and lower
376 reaches of the Yangtze River from June to mid-July and northern and northeastern
377 China from late July to mid-August (Lu et al., 2017; Su et al., 2014; Zhao and Wang,



2017). In our case, with the focus on the association between summer O₃ and WPSH from the interannual perspective, we show that the growing summer rainfall in southern and southeastern China is associated with stronger WPSH in an east position, featured by negative GH composite anomalies to the south of 35°N in China (**Fig. 5a**). Such GH anomaly pattern does not favor atmospheric water vapor transport to North China by the summer monsoon circulations (Nie et al., 2021), which results in low rainfall in this part of China (**Fig. 5c**). Accordingly, relatively higher SATs are observed in North China (**Fig. 5e**), which, together with low atmospheric humidity and rainfall, favors O₃ formation and evolution. On the other hand, the stronger rainfall in southern and southeastern China caused lower SATs in this region, characterized by negative SAT composite anomalies (**Fig. 5e**). The higher atmospheric humidity, stronger rainfall or precipitation washout, and lower SATs tend to restrain O₃ formation in southern China, which resulted in lower O₃ levels compared to that measured in central and northern China (Lu et al., 2018; Liu, 2020). This is likely a reason for higher O₃ concentrations observed in northern and central-north China, such as the BTH and central China urban agglomerations, than in YRD and PRD regions. In the negative phase of the WPSH-I2, the north-south contrast pattern of all three meteorological variables vanished. Instead, positive GH composite anomalies at the 500-hPa are seen in China, with more muscular positive anomalies in western Mongolia (**Fig. 5b**). Such GH pattern suggests the reinforcement and western shift of the WPSH. As a result, the composite anomalies of the summer precipitation in northern China turned to positive, meaning high rainfall in this region (**Fig. 5d**). However, the composite anomalies of SATs in the negative phase of the WPSH-I2 (**Fig. 5f**) seem not to respond well to the intense rainfall, except in the PRD, where declining SATs, featured by the negative SAT composite anomalies (**Fig. 5f**), corresponding well to the positive composite precipitation anomalies, meaning high rainfall in this region (**Fig. 5d**). This result also is in line with previous observations that the westward shift of the WPSH ridge point often accompanied with the termination of the systematic rainfall in southern China (Duan et al., 2008; Huang et al., 2018; Nie et al., 2021).



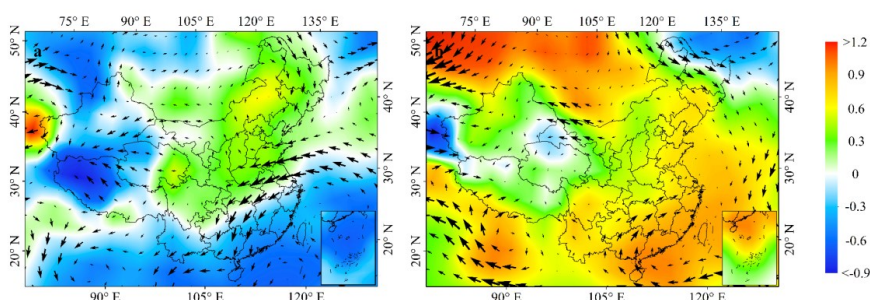
407



408

409 **Figure 5.** Anomalies of composite means of 500-hPa GH (GPH) in positive (a) and negative (b)
 410 phase of WPSH-I2 from 1999 to 2017; same as Fig. 5a and 5b but for precipitation (cm/mm) in
 411 positive (c) and negative (d) WPSH-I2 phase; same as Fig. 5a and 5b but for SAT (°C) in positive
 412 (e) and negative (f) phase of WPSH-I2 from 1999 to 2017.

413



414

415 **Figure 6.** Anomalies of composite means of sea level pressure (SLP, hPa) overlapped with the
 416 anomalies of composite mean 850-hPa vector winds across China in the positive (a) and negative
 417 (b) phases of WPSH-I2 from 1999 to 2017.

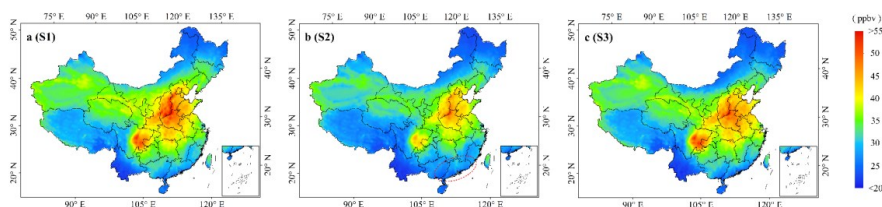
418

419 3.3. WPSH and interannual O₃ fluctuations

420 Having identified the associations between the WPSH and O₃ evolution on
 421 interannual scales, it is also interesting to know to what extent the WPSH could
 422 contribute to the interannual fluctuations in O₃ concentrations in China and its major
 423 urban agglomerations. We compared modeled O₃ concentrations among three model
 424 scenarios by estimating their differences (fractions). **Figure 7** illustrates summer mean



425 O₃ concentrations averaged from 1999 to 2017 from the three scenarios. Identical
 426 concentration spatial patterns can be observed in scenarios 1 (base, **Fig. 7a**) and 3 (fixed
 427 meteorology, **Fig. 7c**), suggesting that precursor emissions overwhelmed the spatial-
 428 temporal distribution of summer ozone in China. Comparing **Figs. 7b** with **Fig. 7a** and
 429 **7c**, we also notice that the low summer ozone levels simulated from model scenario 2
 430 (fixed precursor emissions, **Fig. 7b**) extend a much larger area across southern China
 431 (highlighted by a solid red circle). Considering that model scenarios 1 and 2 used the
 432 same meteorological data from 1998 to 2017, the lower O₃ levels under scenario 2 can
 433 be attributed mainly to declining precursor emissions, partly attributable to a
 434 collaborative effort to mitigate air pollution in the PRD and Hong Kong since the early
 435 2000s as aforementioned before, which effectively slowed down growing O₃ precursor
 436 emissions (Wu et al., 2013).
 437



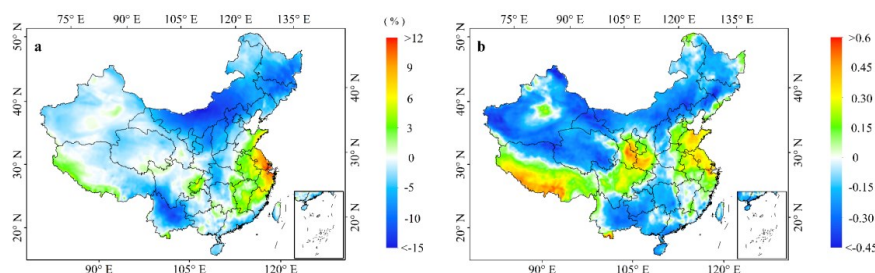
438
 439 **Figure 7.** Modeled mean summer O₃ concentrations across China averaged from 1999 to 2017: (a)
 440 Model scenario 1 (base scenario), (b) model scenario 2 (fixed precursor emission), and (c) model
 441 scenario 3 (fixed meteorology).
 442

443 To extract signals of meteorology in modeled O₃ concentrations, we calculated the
 444 percentage change in summer O₃ concentrations subject to model scenarios 1 and 3,
 445 defined as $O_{3, \text{frac}} = (O_{3(S3)} - O_{3(S1)}) / O_{3(S1)} \times 100\%$, where $O_{3(S3)}$ and $O_{3(S1)}$ represent the
 446 summer ozone concentrations for scenarios 3 and 1 between 1999 and 2017 (**Fig. 8a**).
 447 Since both model scenarios 1 and 3 used the same precursor emissions, their differences
 448 (fractions) can quantify the meteorological effect on O₃ fluctuations. Significantly, the
 449 WPSH was at a relatively high value in 1998 compared to 1999-2017 (**Fig. S2**). The
 450 result shows that the fixed meteorological conditions (scenario 3) resulted in higher
 451 summer ozone concentrations in the eastern seaboard region of China than the results



452 from the base scenario, particularly in the YRD, where the fixed meteorological
453 conditions enhanced the summer concentration by >9% compared to the base scenario
454 modeling result (**Fig. 8a**). The second-highest O₃ fraction between the scenarios 1 and
455 3 occurred in the Sichuan Basin, where the scenario 3 predicted the summer
456 concentrations are 3% to 6% higher than the base scenario 1. **Figure 8b** presents the
457 correlation coefficients between the WPSH-I1 and scenario 2 modeled O₃
458 concentrations across China from 1999 to 2017, showing relatively high positive
459 correlation coefficients in the eastern seaboard area and the region extending from the
460 Sichuan Basin to the Gansu-Shaanxi border, like the fractional changes shown in **Fig.**
461 **8a**. However, the negative correlations extended in most parts of China, indicating that
462 the WPSH tends to reduce summer O₃ levels in these regions. This spatial correlation
463 pattern differs significantly from the correlation pattern shown in **Fig. 4**, in which
464 positive correlations between the summer WPSH and modeled O₃ under the base
465 scenario almost extend entire China. As aforementioned, this is because both WPSH-
466 I1 and O₃ precursor emissions in China increased from 1999 to 2017. **Figure 8** shows
467 some similarities between spatial distribution patterns of the fractional changes in
468 summer O₃ concentrations under scenarios 1 and 3 and the correlations of summer O₃
469 concentrations from model scenario 2 and the WPSHI-I1. The result suggests that the
470 meteorological conditions contributing to summer O₃ evolution, as shown in **Fig. 8a**,
471 are associated, to a large extent, with the WPSH. The positive contribution of
472 meteorology characterized by the positive correlations to elevated O₃ pollution
473 gradually weakens in inland areas and turns into a negative contribution, meaning the
474 reduction of summer O₃ by meteorology in inland China, including most northern and
475 northeastern regions. Although positive correlations were estimated in the Tibet Plateau,
476 given very low O₃ pollution, the WPSH would not exert any significant influence on
477 O₃ levels in the plateau.

478



479

480 **Figure 8.** Fractional changes between modeled O₃ concentrations subject to model scenarios 3 and
 481 1 from 1999 to 2017 estimated by $O_{3,frac} = (O_{3(S3)} - O_{3(S1)}) / O_{3(S1)} \times 100\%$ (a), and correlation
 482 coefficients between summer WPSH-II and modeled summer O₃ concentrations under model
 483 scenario 2 (b).

484

485 As shown in **Fig. 5c**, the positive WPSH-II corresponds to lower precipitation in
 486 southern and southeastern China and higher precipitation in central and northern China,
 487 which tends to enhance O₃ levels in southern and southeastern China and reduce O₃
 488 concentrations in the north. Although we also observe higher SATs across northern
 489 China and lower SATs in the south, which should increase O₃ levels in the north and
 490 decrease O₃ levels in the south, we could not quantify the direct linkages between SATs
 491 and O₃ concentrations from a national perspective. **Figure S9** displays the correlation
 492 coefficients between summer WPSH-II and the SAT (**Fig. S9a**) and precipitation (**Fig.**
 493 **S9b**). We can observe stronger positive correlations between the WPSH-II and SAT in
 494 southern China, indicating that the WPSH tends to enhance SAT in this region. This
 495 should favor elevated O₃ concentrations instead of the reduction of O₃ levels, as shown
 496 in **Fig. 7b**. This result likely anticipates that stronger precipitation associated with
 497 WPSH in this part of China overwhelmed SAT and overall yielded lower O₃
 498 concentrations in southern China.

499 **Figure S10** illustrates annual variations of summer averaged O₃ concentrations
 500 under the three model scenarios from 1998 to 2017 over six UAs. Distinct differences
 501 between the three inland UAs (CY, CC, and MYR) and the three coastal UAs (YRD,
 502 PRD, and BTH) can be discerned from more significant fractions with an increasing
 503 trend in CY, CC, and MYR, as compared to YRD, PRD, and BTH, in which there were



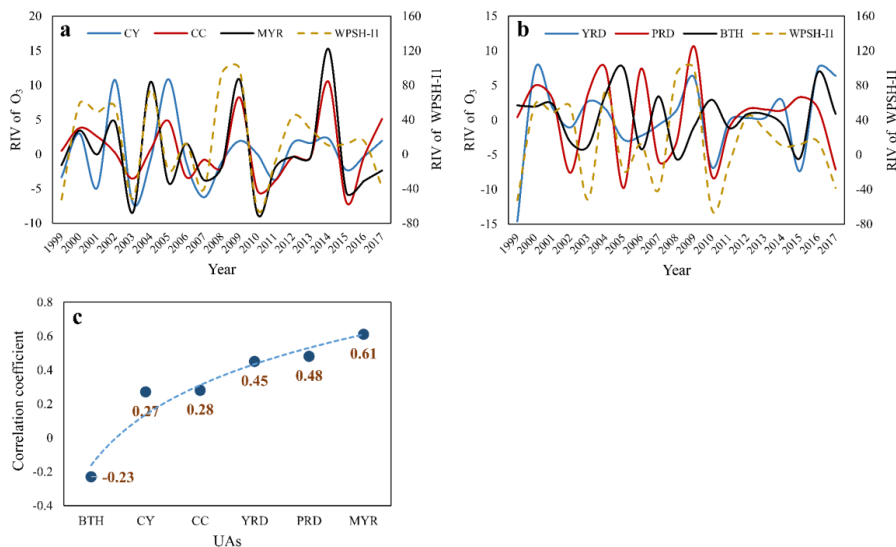
504 no significant trends in modeled concentrations. In the three inland UAs (CY, CC, and
505 MYR, **Fig. S10d-f**), O₃ concentrations under fixed precursor emissions (scenario 2,
506 solid red line) are lower markedly than that from scenario 1 (solid green line) and exhibit
507 no statistically significant temporal trend, suggesting that the variable meteorology
508 does not contribute significantly to O₃ levels and its long-term temporal trends. On the
509 other hand, O₃ concentrations under scenarios 1 and 3 runs are more or less similar and
510 illustrate increasing trends, indicating that growing precursor emissions in the past two
511 decades dominate long-term O₃ evolution in these inland UAs. In the three coastal UAs
512 (PRD, YRD, and BTH), the increasing trends of modeled summer O₃ under scenario 3
513 were less significant than in the three inland UAs, indicating slower growth of precursor
514 emissions in these coastal UAs. No significant increasing trends of O₃ concentrations
515 from scenario 3 run (fixed emission in 1998) are observed, suggesting that the changes
516 in meteorological conditions in the past two decades contributed less to growing O₃
517 pollution in China's major urban clusters than precursor emissions. However, we
518 noticed from **Fig. S10** that annual fluctuations of summer O₃ concentrations in these
519 UAs under scenario 2 agree, to a large extent, with the results from model scenario 1
520 (base scenario). This is expected because the two model scenarios shared the same
521 meteorology. As a result, precursor emissions contributed primarily to the long-term
522 O₃ growing trends and magnitudes, whereas meteorology made more vital
523 contributions to interannual fluctuations of O₃ concentrations.

524 To link the interannual fluctuations of summer ozone induced by meteorology
525 with WPSH, we estimated the rate of interannual variation (RIV) of summer O₃
526 concentrations simulated by scenario 2 in the 6 UAs and WPSH-II, given by $C_r = [c(n)$
527 $- c(n-1)]/c(n-1) \times 100\%$, where $c(n)$ and $c(n-1)$ are summer O₃ concentrations in the
528 current year and previous year, respectively. The same approach also calculated the
529 RIV of summer WPSH-II. **Figures 9a** and **9b** present the RIV of summer O₃
530 concentrations in the three inland and coastal UAs, respectively. The RIV of the WPSH-
531 II is also shown in the figure (brown dashed line). Although these RIVs do not exhibit
532 significant trends, we can observe a general agreement of the RIV between the
533 WPASH-II and summer O₃ concentrations in most UAs, featured by their annual



534 oscillations. **Figure 9c** shows the correlation coefficients between the RIVs of the
 535 summer WPSH-II and O₃ concentrations. The highest correlation is found in the MYR,
 536 followed by the PRD and YRD, whereas the lowest correlation occurred in the BTH.
 537 These correlations suggest that the O₃ interannual fluctuations in those areas proximate
 538 to the WPSH tend to be more strongly associated with the WPSH, regardless of the
 539 positive or negative effect of the WPSH on O₃ evolution. Since the meteorology
 540 determined largely the interannual fluctuations of summer O₃ and connected nicely with
 541 the WPSH, the associations of the RIVs between summer the WPSH-II and O₃
 542 concentrations imply that the WPSH made a more contribution to the interannual
 543 variation of summer O₃, rather than its long-term trend, though the WPSH-II presents
 544 an increasing trend after 1998 (**Fig. 3**).

545



546

547 **Figure 9.** (a) Rate of interannual variations of summer WPSH-II (brown dashed line) and O₃ in CY,
 548 CC, and MYR from 1999 to 2017, (b) same as Fig. 9a but for YRD, PRD, and BTH, and (c)
 549 correlation coefficients of the rate of interannual variations of summer WPSH-II and O₃ in six UAs
 550 from 1999 to 2017.

551

552 **4. Conclusions**



553 Model simulations revealed higher O₃ concentrations from 1999 to 2017 in the
554 Sichuan Basin and the region extending from central China to the NCP, agreeing with
555 measured mean summer concentrations. The first EOF loadings (PCA1) are associated
556 strongly with the mean summer O₃ concentrations across China and its major UAs. We
557 identified distinctive differences between positive and negative WPSH anomalies and
558 elucidated their impacts on interannual variation of O₃ and meteorological conditions.
559 In some of the UAs, such as the PRD, where relatively lower O₃ levels were reported
560 compared to other major UAs, the WPSH tended to reduce O₃ levels. The EOF and
561 regression analysis revealed stronger responses of summer O₃ in the region extending
562 from southeastern to central China. We noted that WPSH became stronger since the late
563 1990s and early 2000s, featured by the enhancing WPSH index after 1999. As a result,
564 stronger associations between summer O₃ in China and its primary UAs and the WPSH
565 occurred in the recent two decades. Extensive model scenario simulations indicated that
566 precursor emissions dominated the long-term trend and magnitude of summer ozone
567 concentrations. However, the meteorology associated with the WPSH largely
568 determined their interannual fluctuations from 1999 to 2017. Our results concluded that
569 the influence of precursor emissions on the evolution of ozone was stronger in
570 Chengdu-Chongqing, the middle reaches of the Yangtze River, and central China than
571 in the coastal city clusters. However, the influence of meteorological conditions is not
572 significant. In contrast, for the coastal city clusters of the Yangtze River Delta, the Pearl
573 River Delta, and the Beijing-Tianjin-Hebei region, the influence of precursor emissions
574 on the summer ozone evolution is weaker than in the inland city clusters, but the
575 influence of meteorological conditions was greater than in the inland city clusters,
576 particularly in those urban areas proximate to the WPSH. Considering the great efforts
577 in China to mitigate O₃ pollution via reducing anthropogenic precursor emissions,
578 interannual and longer-term O₃ evolutions associated with increasing WPSH strength
579 might be worth paying attention because it might influence background O₃
580 concentration, its long-term prediction, and long-term O₃ mitigation measures. The
581 results from the present study might also imply that the local policy makers in different
582 UAs should take the WPSH's impacts into account in making their respective O₃



583 reduction strategies, in addition to precursor emissions. To the end, it is worth noting
584 that this modeling study was partly based on an increasing trend of the summer WPSH
585 strength since 2000, which coincided with growing O₃ evolution. Historically, the
586 WPSH has been fluctuated on a yearly basis. Further study needs to be conducted to
587 discern the associations between projected WPSH and O₃ concentrations subject to
588 future climate change scenarios, such as shared socioeconomic pathways under
589 Coupled Model Intercomparison Project (CMIP6) and the Intergovernmental Panel on
590 Climate Change (O'Neill et al., 2017).

591

592

593 **Code/Data availability**

594 Data will be made available on request.

595

596 **Author contributions**

597 All authors contributed to the manuscript and have given approval of the final version.
598 XZ, RZ and XJ designed the research. XZ, XL and KC collected the data. ST, JL, HG
599 and TH contributed to the interpretation of results. XZ, RZ and JM wrote and revised
600 the manuscript.

601

602 **Competing interests**

603 The authors declare that they have no known competing financial interests or personal
604 relationships that could have appeared to influence the work reported in this paper.

605

606 **Financial support**

607 This study is supported by the National Natural Science Foundation of China
608 (41991312, 41977357).

609

610 **Appendix A. Supplementary data**

611 Supplementary data to this article can be found online

612

613 **References**

614 Akimoto, H., Mori, Y., Sasaki, K., Nakanishi, H., Ohizumi, T., and Itano, Y.: Analysis of monitoring
615 data of ground-level ozone in Japan for long-term trend during 1990–2010: Causes of temporal
616 and spatial variation, *Atmos. Environ.*, 102, 302–310,
617 <https://doi.org/10.1016/J.ATMOENV.2014.12.001>, 2015.

618 Bell, M. L., Zanobetti, A., and Dominici, F.: Who is more affected by ozone pollution? A systematic
619 review and meta-analysis, *American Journal of Epidemiology*, 180, 15–28,



- 620 <https://doi.org/10.1093/aje/kwu115>, 2014.
- 621 Brauer, M., Amann, M., Burnett, R. T., Cohen, A., Dentener, F., Ezzati, M., Henderson, S. B.,
622 Krzyzanowski, M., Martin, R., van Dingenen, R., van Donkelaar, A., and Thurston, G. D.:
623 Exposure assessment for estimation of the global burden of disease attributable to outdoor air
624 pollution, *Environ. Sci. Technol.*, 46, 652–660, <https://doi.org/10.1021/es2025752>, 2012.
- 625 Chen, Z., Li, R., Chen, D., Zhuang, Y., Gao, B., Yang, L., and Li, M.: Understanding the causal
626 influence of major meteorological factors on ground ozone concentrations across China, *J.*
627 *Clean. Prod.*, 242, 118498, <https://doi.org/10.1016/j.jclepro.2019.118498>, 2020.
- 628 Dang, R., Liao, H., and Fu, Y.: Quantifying the anthropogenic and meteorological influences on
629 summertime surface ozone in China over 2012–2017, *Sci. Total Environ.*, 754, 142394,
630 <https://doi.org/10.1016/j.scitotenv.2020.142394>, 2021.
- 631 Ding, D., Xing, J., Wang, S., Chang, X., and Hao, J.: Impacts of emissions and meteorological
632 changes on China’s ozone pollution in the warm seasons of 2013 and 2017, *Front. Environ.*
633 *Sci. Eng.*, 13, 76, <https://doi.org/10.1007/s11783-019-1160-1>, 2019.
- 634 Duan, L., Rong, Y., and Liang, P.: Effect of West Pacific Subtropical High on Summer Precipitation
635 in North China, *Met. Sci. Technol.*, 36, 273–276, [http://www.cnki.com.cn/Article/CJFDTotal-](http://www.cnki.com.cn/Article/CJFDTotal-QXKJ200803004.htm)
636 [QXKJ200803004.htm](http://www.cnki.com.cn/Article/CJFDTotal-QXKJ200803004.htm), 2008.
- 637 Fiore, A. M., Jacob, D. J., Mathur, R., and Martin, R. V.: Application of empirical orthogonal
638 functions to evaluate ozone simulations with regional and global models, *J. Geophys. Res.*
639 *Atmos.*, 108, <https://doi.org/10.1029/2002jd003151>, 2003.
- 640 Fleming, Z. L., Doherty, R. M., von Schneidmesser, E., Malley, C. S., Cooper, O. R., Pinto, J. P.,
641 Colette, A., Xu, X., Simpson, D., Schultz, M. G., Lefohn, A. S., Hamad, S., Moolla, R., Solberg,
642 S., and Feng, Z.: Tropospheric Ozone Assessment Report: Present-day ozone distribution and
643 trends relevant to human health, *Elementa*, 6, 12, <https://doi.org/10.1525/elementa.273>, 2018.
- 644 Fu, Y., Liao, H., and Yang, Y.: Interannual and Decadal Changes in Tropospheric Ozone in China
645 and the Associated Chemistry–Climate Interactions: A Review, *Adv. Atmos. Sci.*, 36, 975–993,
646 <https://doi.org/10.1007/s00376-019>, 2019.
- 647 Guenther, A. B., Jiang, X., Heald, C. L., Sakulyanontvittaya, T., Duhl, T., Emmons, L. K., and Wang,
648 X.: The Model of Emissions of Gases and Aerosols from Nature version 2.1 (MEGAN2.1): an
649 extended and updated framework for modeling biogenic emissions, *Geosci. Model Dev.*, 5,
650 1471–1492, <https://doi.org/10.5194/gmd-5-1471-2012>, 2012.
- 651 Han, H., Liu, J., Shu, L., Wang, T., and Yuan, H.: Local and synoptic meteorological influences on
652 daily variability in summertime surface ozone in eastern China, *Atmos. Chem. Phys.*, 20, 203–
653 222, <https://doi.org/10.5194/acp-20-203-2020>, 2020.
- 654 Huang, Y., Wang, B., Li, X., and Wang, H.: Changes in the influence of the western Pacific
655 subtropical high on Asian summer monsoon rainfall in the late 1990s, *Clim. Dyn.*, 51, 443–
656 455, <https://doi.org/10.1007/s00382-017-3933-1>, 2018.
- 657 Jiang, Z., Li, J., Lu, X., Gong, C., Zhang, L., and Liao, H.: Impact of western Pacific subtropical
658 high on ozone pollution over eastern China, *Atmos. Chem. Phys.*, 21, 2601–2613,
659 <https://doi.org/10.5194/acp-21-2601-2021>, 2021.



- 660 Lefohn, A. S., Malley, C. S., Simon, H., Wells, B., Xu, X., Zhang, L., and Wang, T.: Responses of
661 human health and vegetation exposure metrics to changes in ozone concentration distributions
662 in the European Union, United States, and China, *Atmos. Environ.*, 152, 123–145,
663 <https://doi.org/10.1016/j.atmosenv.2016.12.025>, 2017.
- 664 Li, K., Jacob, D. J., Liao, H., Shen, L., Zhang, Q., and Bates, K. H.: Anthropogenic drivers of 2013–
665 2017 trends in summer surface ozone in China, *Proc. Natl. Acad. Sci. U. S. A.*, 116, 422–427,
666 <https://doi.org/10.1073/pnas.1812168116>, 2019.
- 667 Li, K., Jacob, D. J., Shen, L., Lu, X., de Smedt, I., and Liao, H.: Increases in surface ozone pollution
668 in China from 2013 to 2019: Anthropogenic and meteorological influences, *Atmos. Chem.
669 Phys.*, 20, 11423–11433, <https://doi.org/10.5194/acp-20-11423-2020>, 2020.
- 670 Lin, C. Q., Lau, A. K. H., Fung, J. C. H., Song, Y. S., Li, Y., Tao, M. H., Lu, X. C., Ma, J., and Lao,
671 X. Q.: Removing the effects of meteorological factors on changes in nitrogen dioxide and
672 ozone concentrations in China from 2013 to 2020, *Sci. Total Environ.*, 793, 148575,
673 <https://doi.org/10.1016/j.scitotenv.2021.148575>, 2021.
- 674 Lin, Y., Zhang, L., Fan, Q., Meng, H., Gao, Y., Gao, H., and Yao, X.: Decoupling impacts of weather
675 conditions on interannual variations in concentrations of criteria air pollutants in South China
676 – constraining analysis uncertainties by using multiple analysis tools, *Atmos. Chem. Phys.*, 22,
677 16073–16090, <https://doi.org/10.5194/acp-22-16073-2022>, 2022.
- 678 Liu, H., Liu, S., Xue, B., Lv, Z., Meng, Z., Yang, X., Xue, T., Yu, Q., and He, K.: Ground-level
679 ozone pollution and its health impacts in China, *Atmos. Environ.*, 173, 223–230,
680 <https://doi.org/10.1016/j.atmosenv.2017.11.014>, 2018.
- 681 Liu, J.: Ozone regionalization and evolution characteristics, and meteorological formation
682 mechanism in China from 2013 to 2018, Ph.D. thesis, [http://cdmd.cnki.com.cn/article/cdmd-
683 10300-1021778486.htm](http://cdmd.cnki.com.cn/article/cdmd-10300-1021778486.htm), 2020.
- 684 Liu, Q., Zhou, T., Mao, H., and Fu, C.: Decadal variations in the relationship between the western
685 Pacific subtropical high and summer heat waves in east China, *J. Clim.*, 32, 1627–1640,
686 <https://doi.org/10.1175/JCLI-D-18-0093.1>, 2019a.
- 687 Liu, Y., Liang, P., and Sun, Y.: Characteristics of the Western Pacific Subtropical High and Summer
688 Rainfall Anomalies, *The Asian Summer Monsoon*, 85–95, [https://doi.org/10.1016/B978-0-12-
689 815881-4.00005-6](https://doi.org/10.1016/B978-0-12-815881-4.00005-6), 2019b.
- 690 Liu, Y., and Wang, T.: Worsening urban ozone pollution in China from 2013 to 2017 - Part 1: The
691 complex and varying roles of meteorology, *Atmos. Chem. Phys.*, 20, 6305–6321,
692 <https://doi.org/10.5194/acp-20-6305-2020>, 2020.
- 693 Lu, M. H., Chen, X., Liu, W. C., Zhu, F., Lim, K. S., McInerney, C. E., and Hu, G.: Swarms of
694 brown planthopper migrate into the lower yangtze river valley under strong western pacific
695 subtropical highs, *Ecosphere*, 8, <https://doi.org/10.1002/ecs2.1967>, 2017.
- 696 Lu, X., Hong, J., Zhang, L., Cooper, O. R., Schultz, M. G., Xu, X., Wang, T., Gao, M., Zhao, Y., and
697 Zhang, Y.: Severe Surface Ozone Pollution in China: A Global Perspective, *Environ. Sci.
698 Technol. Lett.*, 5, 487–494, <https://doi.org/10.1021/acs.estlett.8b00366>, 2018.
- 699 Lu, X., Zhang, L., Zhao, Y., Jacob, D. J., Hu, Y., Hu, L., Gao, M., Liu, X., Petropavlovskikh, I.,



- 700 McClure-Begley, A., and Querel, R.: Surface and tropospheric ozone trends in the Southern
701 Hemisphere since 1990: possible linkages to poleward expansion of the Hadley circulation,
702 *Sci. Bull.*, 64, 400–409, <https://doi.org/10.1016/j.scib.2018.12.021>, 2019.
- 703 Ma, M., Yao, G., Guo, J., and Bai, K.: Distinct spatiotemporal variation patterns of surface ozone in
704 China due to diverse influential factors, *J. Environ. Manage.*, 288, 112368,
705 <https://doi.org/10.1016/j.jenvman.2021.112368>, 2021.
- 706 Ma, Z., Xu, J., Quan, W., Zhang, Z., Lin, W., and Xu, X.: Significant increase of surface ozone at a
707 rural site, north of eastern China, *Atmos. Chem. Phys.*, 16, 3969–3977,
708 <https://doi.org/10.5194/acp-16-3969-2016>, 2016.
- 709 Maji, K. J., Ye, W. F., Arora, M., and Nagendra, S. M. S.: Ozone pollution in Chinese cities:
710 Assessment of seasonal variation, health effects and economic burden, *Environ. Pollut.*, 247,
711 792–801, <https://doi.org/10.1016/j.envpol.2019.01.049>, 2019.
- 712 Monks, P. S., Archibald, A. T., Colette, A., Cooper, O., Coyle, M., Derwent, R., Fowler, D., Granier,
713 C., Law, K. S., Mills, G. E., Stevenson, D. S., Tarasova, O., Thouret, V., von Schneidmesser,
714 E., Sommariva, R., Wild, O., and Williams, M. L.: Tropospheric ozone and its precursors from
715 the urban to the global scale from air quality to short-lived climate forcer, *Atmos. Chem. Phys.*,
716 <https://doi.org/10.5194/acp-15-8889-2015>, 2015.
- 717 Nie, J., Liu, P., and Zhao, C.: Research on Relationship between Various Indexes of the Western
718 North Pacific Subtropical High and Summer Precipitation in Eastern China, *Chinese Journal
719 of Atmospheric Sciences*, 45, 833–850, <https://doi.org/10.3878/j.issn.1006-9895.2009.20160>,
720 2021.
- 721 O’Neill, B. C., Kriegler, E., Ebi, K. L., Kemp-Benedict, E., Riahi, K., Rothman, D. S., van Ruijven,
722 B. J., van Vuuren, D. P., Birkmann, J., Kok, K., Levy, M., and Solecki, W.: The roads ahead:
723 Narratives for shared socioeconomic pathways describing world futures in the 21st century,
724 *Global Environmental Change*, 42, 169–180, <https://doi.org/10.1016/j.gloenvcha.2015.01.004>,
725 2017.
- 726 Pu, B., Dickinson, R. E., and Fu, R.: Dynamical connection between Great Plains low-level winds
727 and variability of central Gulf States precipitation, *J. Geophys. Res.*, 121, 3421–3434,
728 <https://doi.org/10.1002/2015JD024045>, 2016.
- 729 Shen, L., Mickley, L. J., and Tai, A. P. K.: Influence of synoptic patterns on surface ozone variability
730 over the eastern United States from 1980 to 2012, *Atmos. Chem. Phys.*, 15, 10925–10938,
731 <https://doi.org/10.5194/acp-15-10925-2015>, 2015.
- 732 Silva, R. A., West, J. J., Zhang, Y., Anenberg, S. C., Lamarque, J. F., Shindell, D. T., Collins, W. J.,
733 Dalsoren, S., Faluvegi, G., Folberth, G., Horowitz, L. W., Nagashima, T., Naik, V., Rumbold,
734 S., Skeie, R., Sudo, K., Takemura, T., Bergmann, D., Cameron-Smith, P., Cionni, I., Doherty,
735 R. M., Eyring, V., Josse, B., MacKenzie, I. A., Plummer, D., Righi, M., Stevenson, D. S., Strode,
736 S., Szopa, S., and Zeng, G.: Global premature mortality due to anthropogenic outdoor air
737 pollution and the contribution of past climate change, *Environ. Res. Lett.*, 8, 034005,
738 <https://doi.org/10.1088/1748-9326/8/3/034005>, 2013.
- 739 Su, T., Xue, F., and Zhang, H.: Simulating the intraseasonal variation of the East Asian summer
740 monsoon by IAP AGCM4.0, *Adv. Atmos. Sci.*, 31, 570–580, <https://doi.org/10.1007/s00376->



- 741 [013-3029-8](https://doi.org/10.5194/egusphere-2023-1373), 2014.
- 742 Wang, Y., Jia, B., Wang, S. C., Estes, M., Shen, L., and Xie, Y.: Influence of the Bermuda High on
743 interannual variability of summertime ozone in the Houston–Galveston–Brazoria region,
744 *Atmos. Chem. Phys.*, 16, 15265–15276, <https://doi.org/10.5194/acp-16-15265-2016>, 2016.
- 745 Wu, D., Fung, J., Yao, T., and Lau, A.: A study of control policy in the Pearl River Delta region by
746 using the particulate matter source apportionment method, *Atmos. Environ.*, 76, 147–161,
747 <https://doi.org/10.1016/j.atmosenv.2012.11.069>, 2013.
- 748 Xu, W., Lin, W., Xu, X., Tang, J., Huang, J., Wu, H., and Zhang, X.: Long-term trends of surface
749 ozone and its influencing factors at the Mt Waliguan GAW station, China-Part 1: Overall trends
750 and characteristics, *Atmos. Chem. Phys.*, 16, 6191–6205, [https://doi.org/10.5194/acp-16-6191-](https://doi.org/10.5194/acp-16-6191-2016)
751 [2016](https://doi.org/10.5194/acp-16-6191-2016), 2016.
- 752 Yan, M., Liu, Z., Liu, X., Duan, H., and Li, T.: Meta-analysis of the Chinese studies of the
753 association between ambient ozone and mortality, *Chemosphere*, 93, 899–905,
754 <https://doi.org/10.1016/j.chemosphere.2013.05.040>, 2013.
- 755 Yang, K., Cai, W., Huang, G., Hu, K., Ng, B., and Wang, G.: Increased variability of the western
756 Pacific subtropical high under greenhouse warming, *Proc. Natl. Acad. Sci. U. S. A.*, 119,
757 e2120335119, [https://doi.org/10.1073/pnas](https://doi.org/10.1073/pnas.2022.03.001), 2022.
- 758 Yihui, D., and Chan, J.: The East Asian summer monsoon: An overview, *Meteorology and*
759 *Atmospheric Physics*, 89, 117–142, <https://doi.org/10.1007/s00703-005-0125-z>, 2005.
- 760 Yin, Z., Cao, B., and Wang, H.: Dominant patterns of summer ozone pollution in eastern China and
761 associated atmospheric circulations, *Atmos. Chem. Phys.*, 19, 13933–13943,
762 <https://doi.org/10.5194/acp-19-13933-2019>, 2019.
- 763 Zhan, Y., Luo, Y., Deng, X., Grieneisen, M. L., Zhang, M., and Di, B.: Spatiotemporal prediction of
764 daily ambient ozone levels across China using random forest for human exposure assessment,
765 *Environ. Pollut.*, 233, 464–473, <https://doi.org/10.1016/j.envpol.2017.10.029>, 2018.
- 766 Zhang, X., Jian, X., Zhao, Y., Liu, X., Chen, K., Wang, L., Tao, S., Liu, J., Huang, T., Gao, H., Liu,
767 Y., Zhugu, R., and Ma, J.: Tropospheric Ozone Perturbations Induced by Urban Land
768 Expansion in China from 1980 to 2017, *Environ. Sci. Technol.*, 56, 6978–6987,
769 <https://doi.org/10.1021/acs.est.1c06664>, 2022.
- 770 Zhao, Z., and Wang, Y.: Influence of the West Pacific subtropical high on surface ozone daily
771 variability in summertime over eastern China, *Atmos. Environ.*, 170, 197–204,
772 <https://doi.org/10.1016/j.atmosenv.2017.09.024>, 2017.
- 773 Zhou, T., Yu, R., Zhang, J., Drange, H., Cassou, C., Deser, C., Hodson, D. L. R., Sanchez-Gomez,
774 E., Li, J., Keenlyside, N., Xin, X., and Okumura, Y.: Why the Western Pacific subtropical high
775 has extended westward since the late 1970s, *J. Clim.*, 22, 2199–2215,
776 <https://doi.org/10.1175/2008JCLI2527.1>, 2009.
- 777